Dispersion interferometer based on a CO_2 laser for TEXTOR and burning plasma experiments

P. A. Bagryansky, A. D. Khilchenko, A. N. Kvashnin,
A. A. Lizunov, and R. V. Voskoboynikov
Budker Institute of Nuclear Physics, Novosibirsk 630090, Russia

A. L. Solomakhin
Novosibirsk State University, Novosibirsk, 630090 Russia

H. R. Koslowski and TEXTOR team
*Forschungszentrum Jülich GmbH, Association EURATOM-FZ Jülich, Institut für Plasmaphysik,
Trilateral Euregio Cluster, 52425 Jülich, Germany*

A dispersion interferometer based on a continuous-wave CO_2 laser source ($\lambda = 9.57$ μm) with double plasma passage for measurements of the line-integrated electron density in the TEXTOR tokamak and the GDT linear system has been developed and tested in experiments. A sensitivity of $\langle n_e l \rangle_{\min} = 2 \times 10^{17}$ m^{-2} and a temporal resolution of 1 ms have been achieved. The interferometer does not need any rigid frame for vibration insulation. Its basic components are installed compactly on an optical bench placed on a stable support outside of the torus. The possibility for the development of a multichannel dispersion interferometer for the next generation of fusion devices (e.g., W7-X, ITER) is discussed. © *2006 American Institute of Physics.* [DOI: 10.1063/1.2202922]

I. INTRODUCTION

Interferometry became a reliable method to solve important physics and engineering tasks in magnetic confinement experiments: measurement and control of both the electron density and the plasma column position. Traditionally, interferometers where the probing and reference channels have different geometrical paths are commonly used for plasma diagnostic. These systems have the basic disadvantage of high sensitivity to vibration and other mechanical instabilities of the interferometer frame.

In order to reduce the influence of vibrations, several solutions are commonly applied:

(1) mounting of optical elements on massive vibration isolation structures (e.g., C-shaped rigid frames encompassing the torus);
(2) use of far infrared probe radiation (118 and 337 μm, see, for example, Ref. 1);
(3) application of two-color interferometers that are combination of two traditional interferometers operating on different wavelengths of probe radiation (see, for example, Refs. 2 and 3).

Solutions (1) and (2) listed above have obvious disadvantages. It will be almost impossible to realize the interferometer system based on a rigid frame on large future devices for burning plasma experiments. This conclusion came from the principal design requirements: the necessity to use labyrinths in neutron shielding blocks mounted in diagnostic ports and the impossibility to use pairs of opposite ports for light guiding. The use of larger wavelengths is constrained by the influence of refraction, since a steep plasma density gradient is a known feature of modern plasma devices. Solution (3) allows one, in principle, to develop a frameless interferometer. Successful attempt to realize the frameless scheme based on a two-color system for ITER was described in Ref. 4. Such a two-colour diagnostic is deemed to be quite complicated, and the task of finding simpler and more cost effective alternatives is still important. Here we consider an interferometer system based on nonlinear frequency doubling, which can be used for plasma diagnostics in contemporary fusion devices and possibly in future burning plasma experiments.

The probing and reference channels of a dispersion interferometer[5,6] (DI) have the same geometrical path, but they are separated in frequency. This feature determines the key advantage of the DI: the measured phase difference is determined, in principle, only by the dispersion of the medium and independent on the interferometer path length.

The basic DI layout consists of two optical frequency doublers (see Fig. 1). The plasma volume is located between both doublers. The probe radiation with the frequency ω is partially converted into the second harmonic (SH) by the first frequency doubler FD1. The two waves with the frequencies ω and 2ω propagate through the medium along the same path. In the second frequency doubler FD2 the component of the probing wave with the fundamental frequency ω is converted into SH, too. The remaining component at fundamental frequency is rejected by the frequency selective filter SF. Thus, the signal recorded by the photodetector (PH) results from the interference between both SH waves. One of them is generated in the first frequency doubler FD1 before entering the plasma, and the second one is generated in FD2 after passage of the plasma. The recorded signal takes the following form:
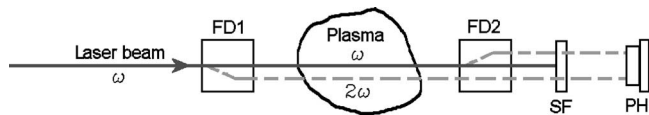
FIG. 1. Principal scheme of the DI: FD1 and FD2—frequency doublers; SF—selective light filter; PH—photodetector; solid line—probe radiation; dashed line—second harmonic radiation.

$$U(\theta) \sim I_{2\omega} = I_1 + I_2 + 2(I_1 I_2)^{1/2} \cos(\theta), \quad (1)$$

where I_1 and I_2 are the beam intensities of the SH radiation produced in FD1 and FD2, respectively, and θ is the phase difference between both interfering waves. The phase difference θ is the difference of the doubled phase of the fundamental wave (due to conversion in the second frequency doubler) and the phase of the SH wave generated in the first doubler,

$$\theta = 2\varphi_1(\omega) - \varphi_2(2\omega) = \frac{2\omega}{c} \int [n(\omega) - n(2\omega)] dl, \quad (2)$$

where $n(\omega)$ is the refractive index of the plasma, and the integration is performed over the coordinate along the beam path. Thus, the attractive feature of the DI is that only the dispersion relation of the medium determines the measured phase difference.

The mentioned feature is particularly useful for DI applications in plasma diagnostics, where the dispersion of the refractive index is governed mainly by the interaction between the probing wave and the electron component of the plasma. Using the well known expression for the refractive index of a plasma,

$$n(\omega) = 1 - \frac{2\pi n_e e^2}{m\omega^2},$$

(n_e is the electron density, e and m are electron charge and mass, and ω is the probing wave frequency) yields the following simple equation for the phase shift:

$$\Delta\theta = \frac{3e^2}{2mc^2} \lambda \langle n_e l \rangle, \quad (3)$$

where λ is the probing radiation wavelength, and $\langle n_e l \rangle$ is the line-integrated electron density. We should note that the above mentioned scheme is only weakly sensitive to changes of both the distance between the frequency doublers and vibrations of optical elements, because air and optical windows have a low dispersion. For a wavelength in the range of $1-10$ μm, the difference $[n(\omega) - n(2\omega)]$ is 4×10^{-8} for air and 1.5×10^{-2} for ZnSe.

A dispersion interferometer based on a Nd:YAG (YAG denotes yttrium aluminum garnet) laser ($\lambda = 1.06$ μm) was developed and successfully used for nuclear fusion experiments.[7–9] However, it is advantageous to use a longer wavelength in the CO_2 emission region (≈ 10 μm) to gain a higher sensitivity to plasma dispersion and a lower sensitivity to coatings of windows and mirrors placed inside the vacuum vessel of the device.

This article describes a DI based on a continuous-wave CO_2 laser. A single-channel prototype of the interferometer was developed for measurements of the line-integrated elec-
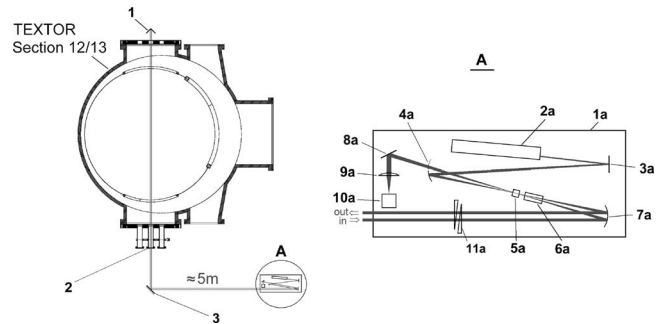

FIG. 2. Dispersion interferometer on TEXTOR: 1—hollow retroreflector; 2—BaF_2 window ($d = 1.5$ in.); 3—additional turning mirror. A: optical bench with DI elements. 1a—optical table; 2a—CO_2 laser; 3a—plane mirror; 4a—half mirror ($r = 0.5$ m); 5a—frequency doubler crystal; 6a—electro-optic cell; 7a—mirror ($r = 1$ m); 8a—plane mirror; 9a—focusing lens; 10a—photo detector; 11a—optical wedge.

tron density in the TEXTOR tokamak (FZ Jülich, Germany) and the GDT mirror device (Budker Institute, Russia). The DI was successfully tested in various experiments. A sensitivity of $\langle n_e l \rangle_{\min} = 2 \times 10^{17}$ m^{-2} and a temporal resolution of 1 ms have been achieved. The main advantages of the dispersion interferometer, such as high sensitivity to plasma dispersion and low sensitivity to vibrations, allowed realizing the optical layout with double plasma passage utilizing a corner cube retroreflector. The optical elements of the DI are installed on a compact optical bench placed outside the plasma torus.

This article is structured as follows. Section II describes the optical system of the newly developed interferometer. Electronics for control and data acquisition systems and the algorithm of the phase calculation are presented in Sec. III, and results of line-integrated electron density measurements in TEXTOR are described in Sec. IV. The results will be discussed in Sec. V.

II. OPTICAL SYSTEM

A schematic drawing of the optical system of the DI mounted on TEXTOR is shown in Fig. 2. Two mirrors (3a and 4a) focus radiation from the CO_2 laser (2a) on to the nonlinear crystal (5a) which converts the radiation at the fundamental frequency partially to the second harmonic. The dimensions of the $ZnGeP_2$ nonlinear crystal are $5 \times 5 \times 5$ mm^3. The beam containing radiation at both wavelengths is then directed to the spherical mirror (7a) which adjusts the beam waist to allow travelling a long distance without any significant change of diameter. The laser beam then passes through two optical wedges (11a). Their function is to tune the interferometer to the maximum of sensitivity. Mirror (3) is used to reflect the beam into the TEXTOR vacuum vessel through a plane-parallel BaF_2 window (2) which has a wedge of $<20''$. After passing once through the plasma, it is reflected by a hollow corner cube reflector (1). The incident beam is displaced relative to the center of this reflector. Consequently, the reflected beam does not coincide spatially with the incident beam but propagates in parallel through the optical system in the reverse direction. After the second passage through the plasma the beam enters again the nonlinear crystal where the remaining fundamental harmonic

radiation is partially converted to the second harmonic. As a result, the beam contains three components of radiation: the first harmonic, the second harmonic produced before the first passage through the plasma, and the second harmonic produced after the second passage through the plasma. A mutual lateral displacement of the forward and backward beams allows the backward beam to be separated from the forward beam on the focusing mirror (4a), which was cut into two equal parts and one half was removed. The forward beam is focused onto the crystal by the half mirror, whereas the backward travelling beam passes through the space corresponding to the removed half of the mirror and is focused by lens (9a) onto the photodetector (10a). The entranc window made of sapphire (Al_2O_3) is used to absorb the radiation at the fundamental frequency. Almost all optical elements are arranged on the optical table (1a), except the retroreflector, which is attached to the upper diagnostic port outside the vacuum chamber (see Fig. 2), and mirror (3) which is attached to the transformer yoke.

A photodetector (10a) (model PDI-2TE-5, VIGO System S.A., Warsaw) with a double-stage Peltier cooling element measures the intensity of the SH radiation. This detector has its maximum spectral sensitivity close to the second harmonic wavelength (≈ 5 μm).

Careful numerical simulation of the optical setup of the DI has been performed prior to assembly. All calculations were performed in the approximation of Gaussian beams. The focal lengths of concave mirrors (4a and 7a) have been intentionally chosen significantly larger than the optimum values for maximum efficiency of radiation conversion to the second harmonic. This was done in order to extend the lifetime of the frequency doubler and to reduce the geometrical shift between the second-harmonic radiation and the fundamental wave. According to the results of the calculations, the laser output power of 15 W at the fundamental frequency yields a second-harmonic radiation power at the photodetector input aperture of about 1 mW, which is sufficient for detection with acceptable signal to noise ratio.

Note that the second-harmonic beam coming back from the plasma could, in principle, generate the fourth-harmonic frequency when it passes the nonlinear crystal again. However, the intensity of the fourth harmonic is negligible. The nonlinear generation of higher harmonics has a resonance nature and the phase-matching condition necessary for efficient generation of fourth-harmonic radiation is not met.

III. CONTROL AND DATA ACQUISITION

A. Phase modulation method

The optical system described in the previous section is designed for measurements of the second-harmonic radiation intensity in the interference field. The photodetector records a signal proportional to the sine of the phase shift in the plasma. Since the sine is not a monotonic function, the phase change can be reconstructed unambiguously only within the limited region of the linear plasma density where the sine of the phase change remains monotonic. This would restrict the range of applicability of the interferometer to measurements of line-integrated electron densities smaller than 10^{19} m^{-2}.
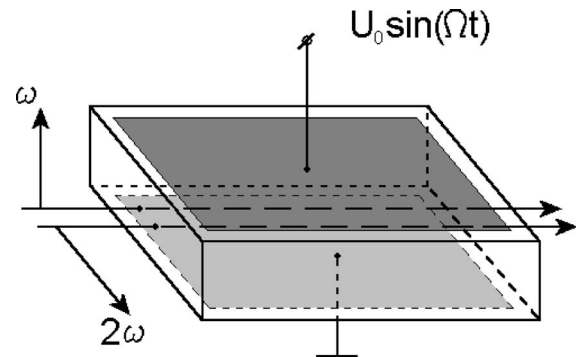

FIG. 3. Electro-optical cell for phase modulation.

In order to overcome this limitation, several improvements of the interferometer scheme and signal processing were introduced. We applied the method of initial radiation phase sweep, which is similar to the well known *zebra stripes* method.[10] An electro-optical cell (EOC, 6a, in Fig. 2) which modulates the phase incursion for both passing waves of the second harmonic with a frequency $\omega = 250$ kHz was placed in the beam path. The basic element of the electro-optical cell (see Fig. 3) was a 50-mm-long GaAs crystal with transverse dimensions of 10×5 mm^2. In its ordinary state, GaAs has a cubic crystal lattice and it is isotropic for radiation. When an electric field is applied to the crystal, it acquires the properties of a biaxial crystal due to the electro-optical effect. The crystal is cut in a way that, upon the application of an electric field, the principal axes of the ellipsoid of the crystal refractive index are oriented in the following manner: along the electric field, along the radiation-propagation direction, and perpendicular to these directions. The refractive index for waves polarized along the electric field remains constant (as in an isotropic crystal); for a wave polarized perpendicular to the electric field the refractive index changes proportional to the electric field strength. Since the first and second harmonics are polarized in perpendicular directions, setting the crystal orientation as shown in Fig. 3 allows shifting the phase proportionally to the electric field for the second harmonic fraction only.

The EOC was manufactured by Elan Co. (St. Petersburg). An antireflection coating for both wavelengths was deposited on both faces (10×5 mm^2) which are traversed by the laser beam. Electrodes were attached to the 10×50 mm^2 faces using a vacuum deposition technique. A sine voltage with a frequency of 250 kHz and an amplitude of about 2.5 kV is applied to the EOC. This voltage corresponds to an additional phase shift of π (half-wavelength voltage).

It is important to note that measurements using this scheme of the interferometer layout with an electro-optical element do not require tuning of the initial phase. Accordingly, the installation of the optical wedges is not necessary anymore, leading to a further reduction of radiation losses due to reflections. The applied phase reconstruction algorithm is described in more detail in Sec. III C.
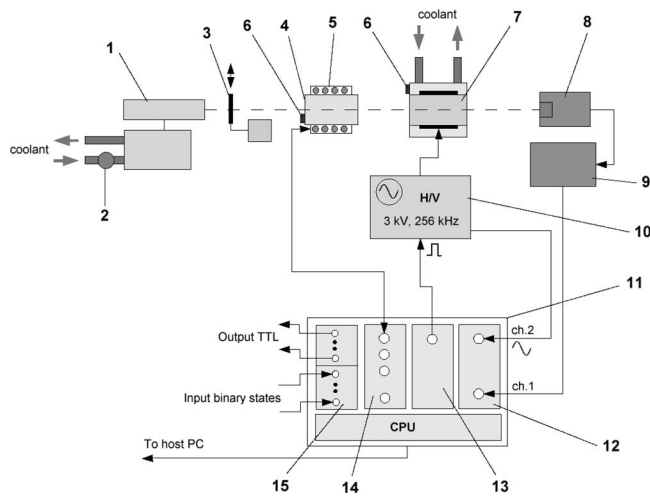
FIG. 4. Block diagram of the interferometer control system: 1—laser; 2—coolant flow sensor; 3—beam shutter; 4—frequency doubler crystal ZnGeP$_2$; 5—heater; 6—temperature sensor; 7—GaAs crystal (EOC); 8—photodetector; 9—detector controller; 10—high-voltage generator for EOC; 11—integrated control module; 12—two-channel 12 bit ADC; 13—reference generator; 14—temperature control and stabilization unit; 15—input/output module.

B. Control system of the dispersion interferometer for TEXTOR

The DI described above is a complex diagnostic system incorporating various optical, electronic, and mechanical elements. A dedicated system was developed to control these elements, to establish the required operating conditions for the active DI modules, to monitor the parameters, and to record the signals.

Figure 4 shows a block diagram of the main elements of the DI and the control system. The main electronic unit is manufactured as an integrated module consisting of monitoring devices, control elements and meters, and remote sensors. The core of the system is an integrated controller based on the ARM7TDI microprocessor. The electromechanical shutter (3) serves to shut off the CO$_2$ laser beam after completion of the measurement sequence. The nonlinear frequency doubler crystal (4) must be kept at a constant temperature with high accuracy, because the refractive indexes strongly depend on temperature. Changes in the refractive indexes lead to changes in both the intensity of conversion and the phase shift for both harmonics and thus contribute directly to the systematic measurement error. The DI control system includes a temperature control and stabilization module (14) which is connected to the crystal heater (5) and several temperature sensors (6) which monitor the temperatures of the nonlinear crystal (7) and the cooling water. The heater maintains the optimum operating crystal temperature of 90 °C within 0.5 °C.

The control system contains a high-voltage ac power supply (10) for generating a modulated voltage for the EOC. A "sync" signal from the reference generator (13) is used for the precise locking of the phase of the modulating voltage to the clock periods of the control system timer. This signal is fed to one channel of the amplitude-to-digital converter (ADC, 12). The signal from the photo detector (8) is digitized in the other ADC channel. The 12 bit ADC has a sam-

pling frequency of 32 MHz. With the total memory capacity of 256 MB, the maximum duration of the measurement amounts to 2 s.

Figure 4 also shows a unit (15) containing binary input registers for monitoring on/off states of modules and TTL (transistor-transistor-logic) output registers for controlling the DI equipment.

The core of the control and data acquisition unit (11) is a processor module incorporating an embedded Ethernet-100 integrated controller. It has a flash memory on board with a preinstalled μClinux operating system.[11] This is actually a high-performance microcomputer that executes a programmed control sequence during experiments. The design of this module permits to operate in heavy-duty conditions, for example, in a noisy environment.

The operator interface of the DI control system is hosted in a so-called upper level computer, which can run under the control of either a Windows or Linux operating system, the latter system was used for the work presented here. In addition to a text-oriented or window interface for controlling the DI, tools for visualization of the measured signals and data archiving were installed on the host computer. In the experiments on TEXTOR an operational mode with automated data processing and uploading the data to the experiment database was successfully tested.

C. Calculation of the line-integrated electron density

The application of the phase modulation technique allows for a simple calculation of the phase shift in the plasma which is a direct measure of the line-integrated electron density. After the passage through the electro-optic cell, the phase of the second harmonic acquires an additional shift $\Delta\varphi_{2\omega}=2kln_{2\omega}[1+g\sin(\Omega t)]$, where k is the wave number, l is the crystal length (50 mm), Ω is the modulation frequency, and g is equal to π for a suitable chosen modulation voltage ($\sim$2.5 kV) applied to the EOC. An oscillating term proportional to the additional phase modulation from the EOC is added to the phase difference between both second-harmonic waves:

$$U_{\text{det}} \propto I_1 + I_2 + 2\sqrt{I_1 I_2}\sin[g\sin(\Omega t)+\varphi].$$

For a certain amplitude of this oscillating term, the interferometer signal changes between the maximum and the minimum of the interference pattern.

A straightforward method for the phase calculation works as follows:

(i)   The time traces of the EOC modulation voltage and the photodetector signal are synchronously digitized.

(ii)   Since the detector signal has the form $A+B\sin(\theta)$, where A and B are assumed to remain constant during one phase modulation period, a constant offset is subtracted from the signal in each period, and the signal is normalized to unity.

(iii) The points where the EOC voltage is zero are determined, and the arcsine of the signal is calculated at these times.

(iv)   The quadrant where the phase is located is determined by analyzing the sign and derivative of the signal from the photodetector, yielding the complete phase information.

(v)   The line-integrated plasma density $\langle n_e l \rangle$ is calculated using formula (3).

The temporal resolution of the measurements is limited by the modulation voltage period (4 μs). The line-integrated electron density is assumed to be constant during one modulation period.

The data acquisition system can be operated in two different modes:

(1)   The signals are digitized and stored in the on-board memory of the control module. After the measurement sequence is finished, the data are transferred to the host personal computer (PC) via Ethernet, and the data are processed by the algorithm described above. The main disadvantages of this regime are (i) no real-time signal processing and (ii) the necessity to transfer large data volumes between the control module and the host PC.

(2)   The phase calculation algorithm is partially coded in the programmable matrix firmware in the DI control module. In this case the processing time, transferred data volumes, and Ethernet connection load are significantly reduced.

Under real experiment conditions, neither the amplitude A of the shift term nor the amplitude B of the sine term is constant. Accordingly, it is important to provide a proper analysis of the stability of the algorithm against changes of these values, taking the modulation period as a characteristic time. This analysis yields the following results:

(1)   A change of A by 1% relative to B leads to an error of $\delta_{err} \approx 10^{17}$ m^{-2}. A change of A by 10% leads to $\delta_{err} \approx 4 \times 10^{17}$ m^{-2}.

(2)   A change of B by 1% relative to its initial value also leads to $\delta_{err} \approx 10^{17}$ m^{-2}. A change of B by 10% leads to $\delta_{err} \approx 2 \times 10^{17}$ m^{-2}.

Obviously, in order to achieve the anticipated accuracy of measurement being better than 10^{17} m^{-2} both relative changes must remain below 1%.

A noise component of the signal also leads to a significant loss of the final accuracy. We simulated the noise by an additional broad-spectrum signal with the relative amplitude of 1%, which can be estimated as an upper noise level. The estimated errors are $\delta_{err} \approx 3 \times 10^{17}$ m^{-2} for phases corresponding to linear sectors (phases close to $n\pi$) and can be up to $\delta_{err} \approx 10^{18}$ m^{-2} for phases close to $\pi/2 + n\pi$. From these results one can conclude that an accurate analog filtering of the recorded signals is mandatory.

As it will be demonstrated below in Sec. IV, the application of a phase detection system allowed for a substantial increase of the measurement accuracy for the line-integrated electron density, compared to the simplest method of phase calculation by measuring the amplitude of the interference term only.
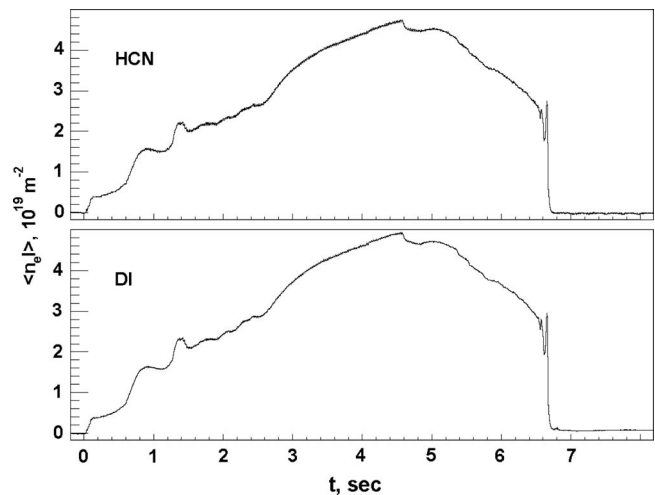

FIG. 5. Signals of the line-integrated electron density in TEXTOR discharge 96042: measured by the dispersion interferometer (lower curve) and by the HCN interferometer (upper curve).

IV. MEASUREMENTS OF THE ELECTRON DENSITY ON TEXTOR

The dispersion interferometer described in the previous section has been installed on the TEXTOR tokamak as shown in Fig. 2. The optical table was located in the TEXTOR basement requiring only one additional mirror mounted at the transformer yoke (see Fig. 2) to guide the probing beam into the torus. Figure 5 shows an example of a time trace of the line-integrated electron density measured with the DI data and for comparison the signal from the central channel of the HCN-interferometer,[12] which measures along a vertical path at almost the same radial location. Any deviations between both signals are small and can probably be explained by the small difference in radial location of the probing beams of both diagnostics. Figure 6 shows a magnified part of the DI line-integrated density signal recorded in the same discharge (No. 96042). The signal clearly resolves the sawtooth oscillations of the electron density. The measurement accuracy achieved under real experimental
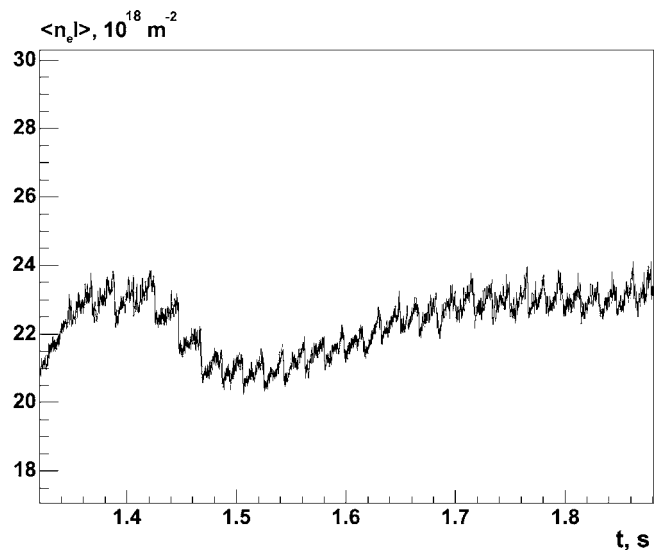

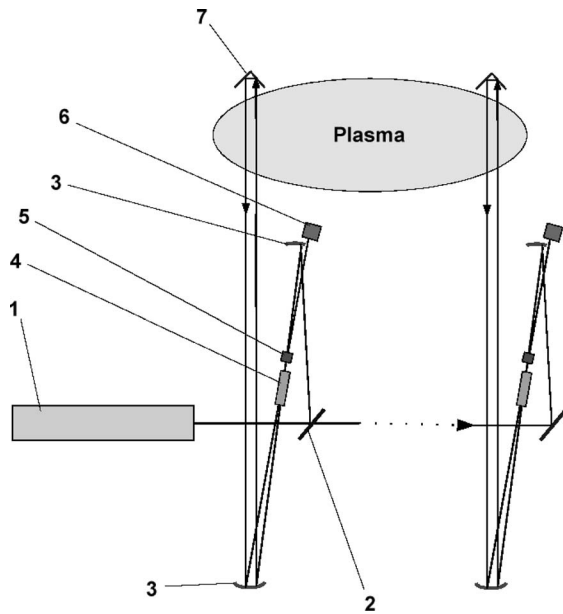FIG. 6. Part of the DI signal showing sawtooth oscillations clearly resolved.

FIG. 7. Principal layout of a DI with several spatial channels: 1—CO$_2$ laser; 2—divider plate; 3—mirror; 4—electro-optic cell; 5—frequency doubler; 6—detector; 7—retro reflector.

FIG. 8. Block diagram of the real-time data processing.

conditions can be estimated to be $\Delta\langle n_e l\rangle \approx 2\times10^{17}$ m^{-2}, and the temporal resolution is about 1 ms. Increasing the temporal resolution for the measurement of sawtooth crashes to 100 μs resulted in a slightly worse $\Delta\langle n_e l\rangle$. In this experiments averaging of raw signals to reduce the noise level has been applied, accordingly the experimental temporal resolution is less than the theoretical maximum of 4 μs, which is achievable for the phase modulation frequency of 250 kHz.

The shorter wavelength of the CO$_2$ laser and its second harmonic reduce the probability of phase jumps considerably. Compared to, e.g., the HCN laser interferometer on TEXTOR phase shifts are more than a factor of 30 smaller. Transient perturbations (such as pellets) will lead to much smaller phase changes which are well below π and will not cause phase jumps. In addition, the phase detection algorithm applied is able to tolerate a complete loss of signal and recover the correct phase reading as long as the change of phase during this time interval remains less than π.

V. SUMMARY AND DISCUSSION

The prototype of a DI for application on toroidal confinement devices has been designed, constructed, and successfully tested on the TEXTOR tokamak. The achieved accuracy and temporal resolution are sufficient to allow real-time control of the plasma. Based on the developed instrumentation technique and obtained results, the capabilities of a dispersion interferometer based on a CO$_2$ laser for future applications in next generation fusion experiments can be estimated. The main challenge can be expressed as the *development of a dispersion interferometer with several spatial channels for large-scale tokamaks and stellarators.*

The modification of the principal layout of a DI for multichord measurements is quite obvious and it does not require any additional complicated technologies for its realization. Figure 7 illustrates on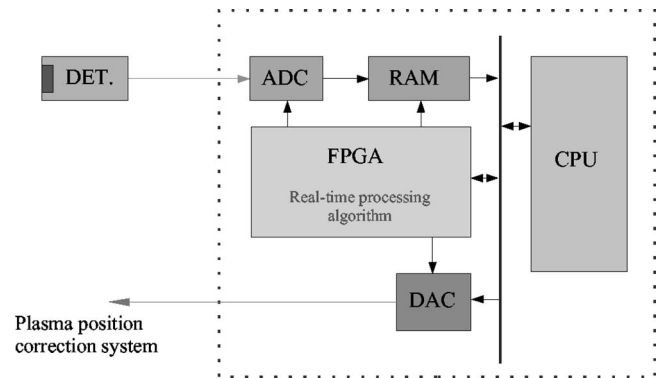e of several possible schemes. A continuous-wave CO$_2$ laser with an output power of 100 W is commercially available for the development of a ten-channel system. The optical setup of each channel can be similar to the one described in this article and it is possible to arrange all the elements on a rather compact optical table. An alternative approach may be to use one less powerful CO$_2$ laser per channel and build independent dispersion interferometer modules.

One important control task in tokamaks is the plasma position detection and feedback control. For this purpose, the signals of line-integrated electron densities from off-axis probing beams arranged symmetrically to the plasma center are analyzed and compared and used to feedback control the currents in the poloidal field coils.[12] This application requires a real-time response from the diagnostic control system. The phase detection method presented in this article is capable to be implemented in a real-time processor. The block diagram of such a real-time processor for the dispersion interferometer is shown in Fig. 8. Within each time frame, the detector signal is digitized and stored in the local memory. The phase reconstruction algorithm is programmed in the field programmable gate array (FPGA). The phase value is calculated and transmitted to the digital-to-analog output (DAC). First estimates show that the full processing sequence can be completed within a time of about 1 ms, fast enough to allow position and density feedback control.

Finally, the DI approach and a two-color interferometer will be compared. As already mentioned in the introduction, a two-color interferometer is a combination of two traditional interferometers where the optical channels have different geometrical paths. Two-color interferometers operate with two different wavelengths of probing radiation. The phase shift measured in each interferometer consists of the phase shift caused by the plasma and the phase shift caused by mechanical perturbations. The signal from the detectors of both interferometers can be expressed as follows:

$$U_{\text{det}}(\Delta\varphi)\propto I=I_1+I_2+2\sqrt{I_1 I_2}\cos(\Delta\varphi_{\text{pert}}+\Delta\varphi_{\text{pl}}),$$

where $\Delta\varphi_{\text{pert}}=2\pi\delta x/\lambda$ is the phase shift caused by mechanical perturbations (δx is the amplitude of perturbation, and λ is the wavelength of probe radiation), and $\Delta\varphi_{\text{pl}}=(e^2/mc^2)\lambda\langle n_e l\rangle$ is the phase shift caused by the plasma. From the mathematical point of view, both unknown quantities $\Delta\varphi_{\text{pert}}$ and $\Delta\varphi_{\text{pl}}$ can be derived from the two independent

measurements. To compare the DI with the two-color system, it is beneficial to calculate the dynamic range d of the phase detection system that is necessary to obtain the required phase resolution $\Delta\varphi_{res} = \Delta\varphi_{pl}/k$, where $k \gg 1$ is the resolution factor:

$$d = \frac{(\Delta\varphi_{pl} + \Delta\varphi_{pert})}{\Delta\varphi_{res}}.$$

After substitution of variables as given above one gets

$$d = k\left(1 + 2\pi\frac{\delta x}{e^2/mc^2}\frac{1}{\langle n_e l\rangle\lambda^2}\right).$$

Note that δx is close to zero for the dispersion interferometer. Taking into account the anticipated ITER parameters: $\langle n_e l\rangle = 10^{21}$ m^{-2}, $\delta x = 1$ mm, and $\lambda = 10$ μm, one can estimate the required dynamic ranges for the phase detection systems of both the DI and the two-color schemes:

$$d = k(1 + 20) \quad \text{two-color interferometer,}$$

$$d = k \quad \text{DI.}$$

Based on this estimate, one can conclude that a considerable higher dynamic range for the phase detection system (or path length stabilization system) of the two-color interferometer is required in order to provide the same phase resolution as the DI.

In summary, the main advantages of the DI in comparison to the two-color system are that (i) the beams of both wavelengths propagate precisely through the same path. This feature is caused by fundamental physics of the second harmonic generation; (ii) the optical system of the DI in a basic setup is much simpler in comparison to a two-color interferometer, and (iii) a much lower dynamic range of the phase detection system is required for a DI than for a two-color scheme to provide the same phase resolution.

ACKNOWLEDGMENTS

[1] H. R. Koslowski and H. Soltwisch, Fusion Eng. Des. **34–35**, 143 (1997).
[2] T. Kondoh, A. E. Costley, T. Sugie, Y. Kawano, A. Malaquias, and C. I. Walker, Rev. Sci. Instrum. **75**, 3420 (2004).
[3] K. Tanaka, A. L. Sanin, L. N. Vyacheslavov, T. Akiyama, K. Kawahata, T. Tokuzawa, Y. Ito, and S. Okajima, Rev. Sci. Instrum. **75**, 3429 (2004).
[4] T. Kondoh, Y. Kawano, A. E. Costley, A. Malaguias, T. Sugie, and C. Walker, *Proceedings of the 30th EPS Conference on Controlled Fusion and Plasma Physics, St. Petersburg*, 7–11 July, 2003 [Europhys. Conf. Abstr. **27A**, P4–64 (2003)].
[5] Kh. P. Alum, Yu. V. Kovalchuk, and G. V. Ostrovskaya, Sov. Tech. Phys. Lett. **7**, 581 (1981).
[6] F. A. Hopf, A. Tomita, and G. Al-Jumaily, Opt. Lett. **5**, 386 (1980).
[7] V. P. Drachev, Yu. I. Krasnikov, and P. A. Bagryansky, Rev. Sci. Instrum. **64**, 1010 (1993).
[8] N. Bretz and F. Jobes, Rev. Sci. Instrum. **68**, 713 (1997).
[9] V. Licht and H. Bluhm, Rev. Sci. Instrum. **71**, 2710 (2000).
[10] M. A. Heald and C. B. Warton, *Plasma Diagnostics with Microwaves* (Wiley, New York, 1965).
[11] www.uclinux. org.
[12] H. Soltwisch *et al.*, Plasma Phys. Controlled Fusion **26**, 23 (1984).